Rev. Mexicana Astron. Astrof., **18**, 65-74 (1989)

EVOLUTION OF H II REGIONS IN DISK-LIKE CLOUDS: THE APPEARANCE OF NEUTRAL HIGH-VELOCITY OUTFLOWS

José Franco[1,2], Guillermo Tenorio-Tagle[2], and Peter Bodenheimer[3]

RESUMEN. Los aspectos mas relevantes en la evolución de regiones H II inmersas en nubes con forma de disco son derivados analíticamente. Las nubes tienen simetría cilíndrica y distribuciones de densidad exponenciales, gausianas y sech^2. Las dimensiones iniciales de las regiones H II son descritas como función del ángulo azimutal θ, en términos del radio de Strömgren para la densidad del plano R_0, y de la escala de altura del disco, H. Cuando $y_0 = R_0\sin(\theta)/H \leq \alpha$ (donde α es una constante que depende de la distribución de densidad), la región H II queda completamente contenida dentro del disco. Para $y_0 > \alpha$ una sección cónica del disco queda totalment ionizada. El ángulo azimutal crítico, arriba del cual la región H II ya no está acotada, está definido por $\theta_{crit} = \sin^{-1}(\alpha H/R_0)$. La expansión de regiones H II que no están acotadas incialmente (i.e., con $y_0 > \alpha$), como fué descrito por Franco *et al.* 1989, se desarrolla principalmente a lo largo del eje z y si la densidad columnar del disco se mantiene constante durante la evolución, el frente de ionización recede y termina siendo atrapado dentro del disco expandido. Cuando las nubes tienen un campo magnético con orientación paralela al eje z, como se esperaría en nubes magnéticas, los efectos del atrapamiento pueden ser muy importantes. El gas expandido y que es afectado por el frente de ionización recedente mantiene su impulso lineal después de recombinarse y es transformado en un flujo neutro de alta velocidad. Si no existe campo magnético, el atrapamiento tiene una duración corta. Algunos otros aspectos adicionales del fenómeno son estudiados con modelos hidrodinámicos en una y dos dimensiones. Los resultado de estos modelos muestran el desarrollo de ondas de choque en los flujos neutros y proveen varios detalles de la etapa de atrapamiento.

ABSTRACT. The main properties of the evolution of H II regions in clouds with disk-like density distributions are derived analytically. The clouds are asummed cylindrically symmetric with exponential, gaussian, and sech^2 density stratifications. The dimensions of the initial H II regions along each azimuthal angle, θ, are described in terms of the Strömgren radius for the midplane density, R_0, and the disk scale heigth, H. For $y_0 = R_0\sin(\theta)/H \leq \alpha$ (where α is a constant dependent on the assumed density distribution) the whole H II region is contained within the disk, and for $y_0 > \alpha$ a conical section of the disk becomes totally ionized. The critical azimuthal angle above which the H II region becomes unbounded is defined by $\theta_{crit} = \sin^{-1}(\alpha H/R_0)$. The expansion of initially unbounded H II regions (*i.e.* with $y_0 > \alpha$), as discussed by Franco *et al.* 1989, proceeds along the z-axis and, if the disk column density remains constant during the evolution, the ionization front eventually recedes from infinity to become trapped within the expanding disk. For clouds threaded by a B-field oriented parallel to the symmetry axis, as expected in magnetically dominated clouds, this effect can be very prominent. The expanding gas overtaken by the receding ionization front maintains its linear momentum after recombination and is transformed into a high-velocity neutral outflow. In the absence of magnetic fields, the trapping has only a short duration. Further particular aspects of the these receding ionization fronts are studied with detailed hydrodynamical numerical simulations of photoionized regions. These show the existence of shocks in the neutral flows and provide more details of the trapping stage.

Key words: **HYDRODYNAMICS – INTERSTELLAR-MATTER – NEBULAE– H II REGIONS**

1. Instituto de Astronomía, Universidad Nacional Autónoma de México.

2. Max-Planck Institut für Astrophysik, Federal Republic of Germany.

3. Lick Observatory, USA

I. INTRODUCTION

The formation and expansion of H II regions in spherical clouds with power-law density distributions and in self-gravitating disks have been recently studied analytically by Franco *et al.* 1989 (hereafter Paper I). This work provides a physical insight to the rich variety of phenomena that can appear during the H II evolution in decreasing density gradients, including the supersonic expansion, the generation of shocks in clouds with power-law density stratifications and, perhaps more remarkable, the existence of receding ionization fronts in self-gravitating disks.

For H II regions expanding in spherical clouds with power-law density profiles, r^{-w}, there is a critical exponent, $w_{crit} = 3/2$, above which the ionization front cannot be "trapped"and the cloud becomes completely ionized. When $w < w_{crit}$, the expansion drives a shock into the ambient medium and the size of the H II region grows with time as $t^{4/(7-2w)}$. The shock collects gas faster than it can be ionized by the photon field, and neutral mass accumulates in the interphase between the ionization and shock fronts. For $w = w_{crit}$, the two fronts move together without mass accumulation (i.e., the gas is ionized immediately after it is shocked), and the expansion velocity is constant at about $2c_i$. Cases with $w > w_{crit}$ become completely ionized and the expansion enters the so-called "champagne"phase (i.e., once the cloud is fully ionized, the expansion proceeds supersonically in the ionized medium). The dense core expands faster than the rest of the ionized cloud and a distinction between two well defined regimes can be made. For $3/2 < w \leq 3$, the slow regime, the core expansion is mildly supersonic and has almost constant velocity. For $w > 3$, the fast regime, the core expansion drives a strongly accelerating shock.

In the case of isothermal self-gravitating disks the density distribution is proportional to $\mathrm{sech}^2(z/H)$ and there exists a critical angle above which the H II region becomes unbounded, $\theta_{crit} = \sin^{-1}(0.88H/R_0)$, where R_0 is the Strömgren radius for the midplane density and H is the disk scale height. This angle corresponds to the direction in which the density gradient becomes steeper than the critical value discussed for spherical clouds and defines a fully ionized conical section in the disk. For initially unbounded H II regions ($y_0 > 0.88$), the gas flows along the z-direction during the early stages of the expansion. The velocities increase with increasing height, up to $z \simeq 2H$, and the disk is stretched with time. For the particular case with $y_0 \simeq 1$ and without magnetic field, the expansion produces a "trapping"stage during which the ionization front is forced to recede from infinity and the H II region becomes ionization bounded. Such a trapping occurs during the early stages of the disk expansion and has a short duration.

Here the study is extended to other types of disk-like density distributions. The approximate effects of magnetic fields directed along the z-axis are also included. Section 2 describes a general formulation for the the initial shape of H II regions embedded in disk-like distributions with exponential, gaussian, and sech^2 density profiles. Section 3 presents the main features of the expansion and the properties of the trapping stage. The basic differences between the magnetic and non-magnetic cases are emphasized. The results of detailed hydrodynamical simulations are presented in Section 4, and a brief discussion is given in Section 5.

II. INITIAL H II REGIONS IN DISK-LIKE CLOUDS

The definition of a "disk-like"cloud is simply an elongated cloud which can be regarded as cylindrically symmetric. The variables r, θ, and z are defined in Figure 1. The gas is assumed molecular with a constant scale height, H, and the ionizing source is located at midplane. The density distribution along the z-axis is

$$n(z) = n_0\, G(z/H), \tag{1}$$

where n_0 is the density at midplane, and $G(z/H)$ is any of the functions $e^{-z/H}$, e^{-z^2/H^2}, and $\mathrm{sech}^2(z/H)$. As discussed in Paper I, power-law profiles with $w > 3/2$ generate unbounded H II regions and, given that the distributions considered here decrease faster than any power-law, there is a critical point for each one of these cases.

The radiation source produces F_* ionizing photons per unit time and generates the H II region. The gas in this H II region is assumed to be fully ionized and, then, the initial ion density is twice the original molecular gas density. The resulting initial size of the H II region is direction dependent and the radius along midplane is (e.g., Osterbrock 1989)

$$R_0 = \left[\frac{3\,F_*}{4\pi(2n_0)^2\alpha_B}\right]^{1/3} \simeq 0.2\, F_{48}^{1/3} n_3^{-2/3} \alpha_0^{1/3}\ pc, \tag{2}$$

where α_B is the hydrogen recombination coefficient to all levels above the ground level, $\alpha_0 = \alpha_B/2.6 \times 10^{-13}$ cm^3 s^{-1}, $F_{48} = F_*/10^{48}$ s^{-1}, and $n_3 = n_0/10^3$ cm^{-3}.

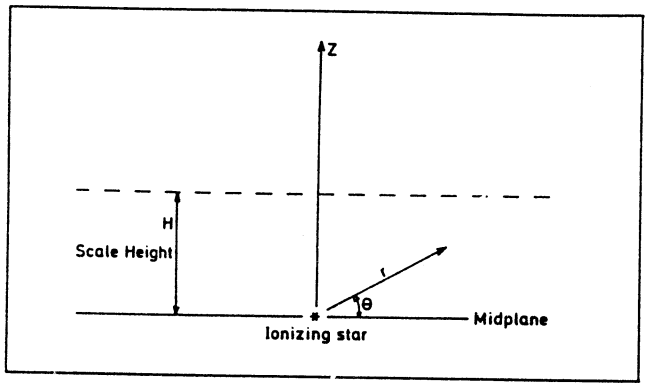

Fig.1. Schematic cross-section of a gaseous disk with a star at midplane.

The initial shape of the ionized region is defined by the equilibrium between photoionization and recombination along each solid angle. Defining the dimensionless variables $y = r\sin(\theta)/H$ and $y_0 = R_0\sin(\theta)/H$, this is obtained by solving the integral equation

$$y_0 = \left[3\int_0^y y^2 G^2(y)\,dy\right]^{1/3}, \tag{3}$$

which is simply the generalization of equation (2) for arbitrary density distributions. As opposed to the constant density case, however, there are no analytical solutions for the integral in the general case. Nonetheless, given the properties of the assumed density stratifications and following the results given in Paper I, the solutions can be approximated by the simple one-parameter fit

$$\left[3\int_0^y y^2 G^2(y)\,dy\right]^{1/3} \simeq \alpha\, tanh(y/\alpha), \tag{4}$$

where $\alpha = [3\int_0^\infty y^2\, G^2(y)\,dy]^{1/3}$ and has the values 0.78, 0.88, and 0.91 for the gaussian, sech^2, and exponential cases, respectively. This fit is selected to match the values of the integral at $y = 0$ and at the critical point (i.e., $y \to \infty$). Thus, the particular functional form of the results presented below depend on the assumed fit but the location of the critical point, θ_{crit}, does not depend on this choice. For $y > 4$ the fit is highly accurate, and for $0 < y < 4$ is better than 5% for the gaussian and sech^2 cases, and better than 17% for the exponential case.

Following the notation of Paper I, the resulting size of the initial H II region as a function of the angle θ can be written as

$$R_\theta \simeq R_0 h(\theta), \tag{5}$$

with the "shape"function

$$h(\theta) = \left(\frac{\alpha}{2y_0}\right) In\left[\frac{1 + (y_0/\alpha)}{1 - (y_0/\alpha)}\right]. \tag{6}$$

For small values of y_0 (i.e., $y_0 \leq 0.3$), the shape function reduces to

$$h(\theta) \simeq \left(1 + \frac{y_0^2}{3\alpha^2}\right). \tag{7}$$

The equivalent average ion mass density along each line of sight weighted by the photoionization process (i.e., the ion density corresponding to a Strömgren radius of size R_θ), is given by

$$\langle \rho_i \rangle = \rho_0 h(\theta)^{-3/2}, \tag{8}$$

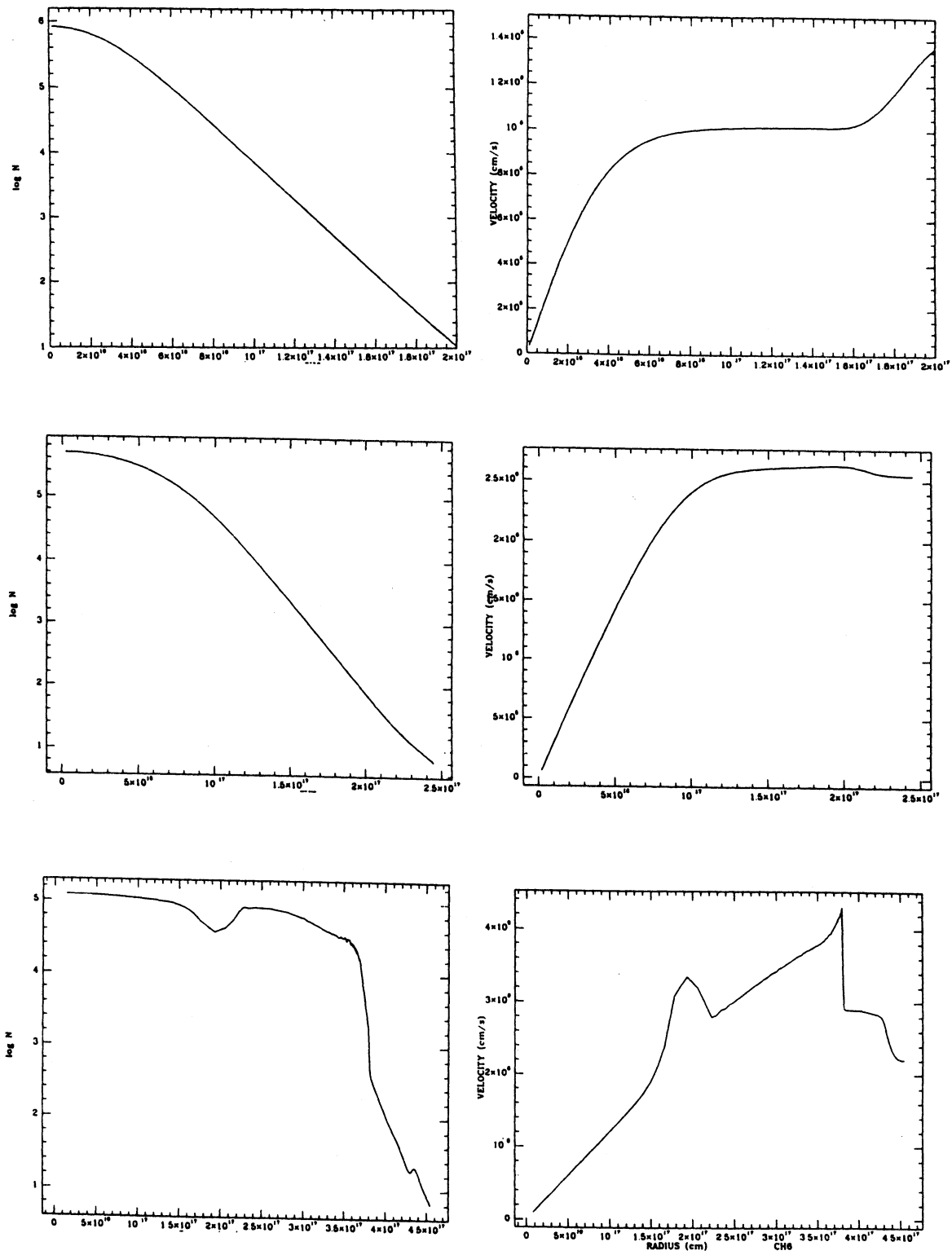

Fig.2. One-dimensional simulation of the expansion of an ionized disk. The density and velocity profiles along the symmetry axis are shown at t = 100 yr, 1 000 yr, and 3 250 yr.

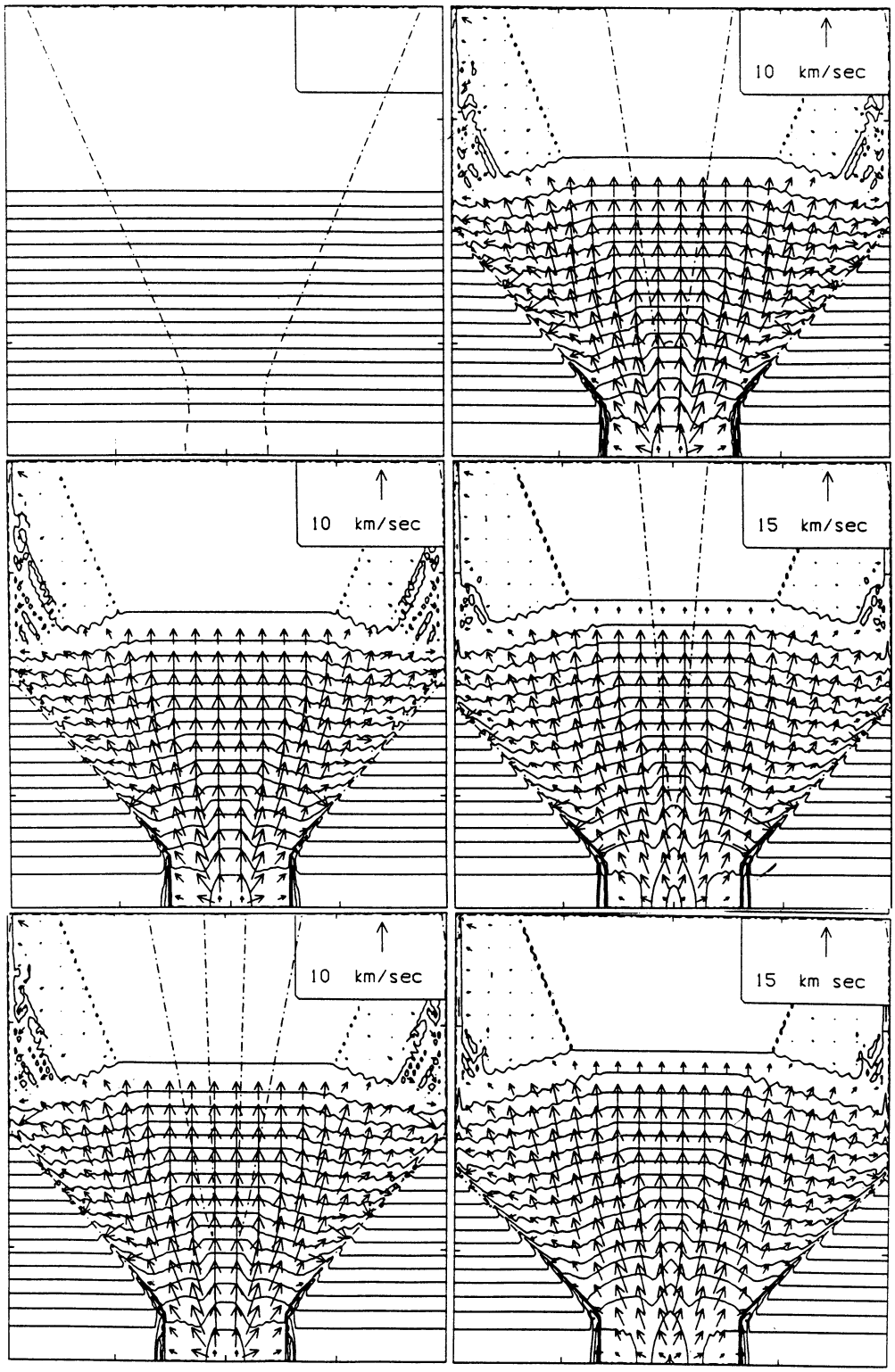

Fig. 3. Two-dimensional simulation of the expansion of an ionized disk. The frames show isodensity contours (solid lines), velocity vectors (arrows), and the location of the ionization front (dashed-dotted lines). The separation in isodensity contours is 0.25 in log ρ, and the value of the unit velocity vector is shown in the right upper corners (in km s^{-1}). The distance between tick marks in the axes is 7.5 $\times$ 10^{16} cm. Frames a-f show the evolution at times t = 0 (the initial condition), 490 yr, 510 yr, 540 yr, 660 yr, and 710 yr, respectively.

where ρ_0 is the mass density at midplane.

The critical point is defined by $y_0 = \alpha$, and this corresponds to a critical angle

$$\theta_{crit} = sin^{-1}\left(\alpha \frac{H}{R_0}\right), \tag{9}$$

which defines the conical section of the disk that is fully ionized and completes the description of the initial stage. Note that the H II region reaches the critical point when $R_0 > \alpha H$, but it becomes completely bounded within the disk when $R_0 \leq \alpha H$. Dust opacity reduces the dimensions of R_0 and R_θ, but the value of the critical point, $y_0 = \alpha$, remains unchanged (see Paper I).

III. THE EXPANSION STAGE: RECEDING IONIZATION FRONTS AND SUPERSONIC NEUTRAL OUTFLOWS

The early stages of the expansion are controlled by the density gradient perpendicular to midplane (see Bodenheimer *et al.* 1983) but, as discussed in Paper I, the details of the general evolution are affected by lateral gas velocity components generated near the boundaries with the neutral gas. These are two-dimensional effects which cannot be treated with a simple analytical scheme. Note, however, that the presence of a B-field oriented in the direction of the disk symmetry axis inhibits the lateral gas movements and the ionized region is forced to expand only along the z-axis. Such a particular disk-field configuration is the one expected in magnetically supported clouds (e.g., Lizano 1989) and allows for a simple one-dimensional treatment of the expansion. For $B = 0$, on the other hand, two dimensional effects become important after a sound crossing time, and this restricts the discussion in the nonmagnetic case to the early stages of the expansion.

The analysis of the magnetic and nonmagnetic cases is performed only along the symmetry axis ($\theta = \pi/2$). The symbols n_0, R_0, H, and y_0 are kept as the initial values (i.e., at $t = 0$) of the corresponding parameters, and the discussion is restricted to initially unbounded regions ($y_0 > \alpha$).

III.1. The expansion with B-fields: high-velocity neutral outflows

The initial gas acceleration is defined by the density gradient

$$a_g(z) \simeq \frac{2zc_i^2}{H^2}, \tag{10a}$$

$$a_s(z) \simeq \frac{2c_i^2}{H} \tanh(z/H), \tag{10b}$$

$$a_e(z) \simeq \frac{c_i^2}{H}, \tag{10c}$$

where c_i is the sound speed in the ionized gas, and the subscripts g, s, and e refer to the gaussian, sech^2, and exponential cases, respectively. These accelerations stretch the whole disk and, as opposed to the power-law case, do not develop shock waves at early times. The gas velocities can, however, reach supersonic values. The magnetic field is assumed uniform and oriented along the z-axis. The flow is constrained to move within the flux tubes and, given that the initial motion is already parallel to z-axis, the main role played by the field is to quench the appearance of lateral motions at later times. Thus, the evolution of the flow can be analysed in one dimension. A rough upper bound to the required field strength at midplane is $B \sim 10^{-4} n_3^{1/2} c_1$ G, where $n_3 = n_0/10^3$ cm^{-3} and $c_1 = c_i/10$ km s^{-1}.

At early times, the location of a gas particle along the z-axis evolves as

$$z(t) \simeq z + a(z)t^2/2, \tag{11a}$$

where z is its original height. In particular, the scale height grows as

$$H(t) \simeq H(1 + \beta c_i^2 t^2/H^2), \tag{11b}$$

with β equal to 1, 0.76, and 0.5 for the gaussian, sech^2, and exponential stratifications, respectively. The expansion changes the density distribution and this change also modifies the gas acceleration. The details of all these variations,

however, are time-dependent and are difficult to treat analytically. Nevertheless, some approximated properties of the flow can be derived with a simple approach.

Mass is conserved along each one of the flux tubes and the column density from midplane to the location of any moving gas parcel remains constant. The column density of half-disk, $N_d = n_0 H$, and the scale height given in equation (11*b*) define the early evolution of the midplane density. Later, as the density gradient in the innermost regions tends to be smoothed out by waves moving with sonic speeds, it can be approximated by $\sim bN_d/(c_i t)$, where b is a factor that matches the evolution at early and late times. There is not a clear cut definition for the transition between these evolutionary stages and, given that the initial density profile is distorted in time scales of the order $\sim 2H/c_i$, we simply define the transition time scale as $\tau_d = 2H/c_i$. Thus, for $t \leq \tau_d$ the midplane density decreases as

$$n_0(t) \simeq n_0(1 + \beta c_i^2 t^2/H^2)^{-1}, \tag{12a}$$

and for $t \geq \tau_d$ it can be approximated by

$$n_0(t) \simeq \frac{n_0 H}{(2\beta + 0.5)c_i t}. \tag{12b}$$

Note that this last equation is equivalent to define a scale height at late times which encloses an almost uniform density and grows as $H(t) \sim (2\beta + 0.5)c_i t$.

Equations (12*a*-12*b*) provide a reasonable approximation for the midplane density, as long as lateral displacements are inhibited, and the size of the H II region along midplane grows approximately as

$$R_0(t) \simeq R_0 \left[\frac{n_0}{n_0(t)}\right]^{2/3} \tag{13}$$

Moreover, at late times (when the density gradient flattens along the z-axis), this is also a representative size of the ionized region in the z-direction. As stated in Paper I, if $R_0(t)$ becomes smaller than $H(t)$, the H II region will be trapped within the expanded disk. Such a trapping results from the dilution of the radiation field and the changes in the density distribution which, however, retains its initial column density. The growth rates for $R_0(t)$ and $H(t)$ are different, and the dimensionless variable $y_0(t) = R_0(t)/H(t)$ is a decreasing function of time. At early times it evolves as

$$y_0(t) \simeq y_0 \left[1 + \beta\left(\frac{c_i t}{H}\right)^2\right]^{-1/3}, \tag{14a}$$

and at late times it is approximated by

$$y_0(t) \simeq y_0 \left[\frac{H}{(2\beta + 0.5)c_i t}\right]^{1/3}. \tag{14b}$$

Thus, there exists a "trapping"time, τ_t, at which the value of $y_0(t)$ drops below unity and the expanding H II region becomes ionization bounded in the z-direction. At this time, which becomes longer with increasing values of y_0, the ionization front recedes down to a location inside $H(t)$ and the gas exterior to this point recombines.

At early times, the effect occurs when the midplane density reaches the value

$$n_0(\tau_t) \simeq (\alpha/y_0)^3 n_0, \tag{15}$$

and the trapping time is defined by

$$\tau_t \simeq \frac{H}{c_i \beta^{1/2}} \left[\left(\frac{y_0}{\alpha}\right)^3 - 1\right]^{1/2}. \tag{16}$$

The constraint $\tau_t \leq \tau_d$ implies that the early times trapping occurs for $y_0 \leq \alpha(4\beta + 1)^{1/3} \sim 1.4$. Therefore, the trapping is delayed to late times when $y_0 \geq 1.4$, and the trapping time is approximated by

$$\tau_t \simeq \frac{H y_0^3}{(2\beta + 0.5)c_i}, \tag{17}$$

when the corresponding midplane density is

$$n_0(\tau_t) \simeq (n_0/y_0^3). \tag{18}$$

After trapping, and as long as the column density remains constant within the flux tubes, the expanding H II region remains ionization bounded. Otherwise, when lateral motions appear and the column density decreases, the H II region becomes again unbounded. This latter case is discussed in the next subsection.

A lower bound to the mass of the recombining zone can be roughly approximated by the mass external to the original scale height

$$M_{rec} \sim \mu\pi R_0^2(\tau_t) n_0 H \int_1^\infty G(x)dx \simeq 0.3\mu\pi R_0^2 y_0^4 n_0 H, \tag{19}$$

where μ is the mass per particle. This gas maintains its momentum after recombination and becomes a neutral high-velocity outflow. Again, a conservative lower bound to its bulk velocity is $\sim 2c_i$. Defining $R_{17} = R_0/10^{17}$ cm, $H_{17} = H/10^{17}$ cm, $c_1 = c_i/10$ km s^{-1}, and $n_6 = n_0/10^6$ cm^{-3}, the lower limits to the mass and momentum locked in the high-velocity neutral flow are $M_{rec} \sim 0.1 R_{17}^2 n_6 H_{17} y_0^4\ M_\odot$ and $P_{rec} \sim 2R_{17}^2 n_6 H_{17} y_0^4 c_1\ M_\odot$ km s^{-1}. These approximate expressions indicate that magnetic cases with $y_0 > 1$ can generate powerful neutral outflows.

III.2. The expansion without B-fields: short trapping stages

In this case, as discussed in Paper I, the expansion leads to lateral gas motions driven by rarefaction waves. These waves reach the z-axis in a sound crossing time, $\tau_{2D} \simeq R_0/c_i$, and the column density begins to decrease afterwards. Thus, the trapping can occur only at the early stages of expansion and its properties are given by equations (15) and (16). The trapping time can be written as

$$\tau_t \simeq \frac{\tau_{2D}}{y_0 \beta^{1/2}} \left[\left(\frac{y_0}{\alpha}\right)^3 - 1 \right]^{1/2}, \tag{20}$$

and the constraint $\tau_t \leq \tau_{2D}$ restricts the existence of the trapping to cases $\alpha < y_0 \leq 1$. Also, given that the gas column density decreases after the rarefaction waves reach the symmetry axis, the trapping is a short lived event and the ionization front moves again outwards after a time τ_{2D}. Thus, for the non-magnetic cases, the H II region will have a variable-size stage shortly after it is born.

IV. NUMERICAL SIMULATIONS

The numerical simulations for the magnetic and non-magnetic cases are performed with one-dimensional and two-dimensional hydrodynamical codes, respectively. The numerical grid resolution in all the models described in this section is 1.5×10^{15} cm, and the ambient gas is assumed atomic.

IV.1. One-dimensional simulations

The one-dimensional hydrodynamical code is described by Tenorio-Tagle *et al.* 1986). The simulations were performed under the assumption of slab symmetry, with a set up representing the density stratification along the symmetry axis. The radiative transport was solved under the assumption of spherical symmetry. Several numerical experiments were performed with different types of density profiles (i.e., gaussian, exponential, and sech^2) and with a variety of midplane densities, scale heights, and photon fluxes. As stated also in Paper I, these runs corroborated the limits for initially unbounded H II regions (when $y_0 > \alpha$), and the approximate properties of the trapping stage (equations 15-18). Similarly, various of these initially unbounded cases were evolved up to 20 times longer than the trapping time and some additional effects were found, in particular, the appearance of a shock front which evolves into the recently recombined gas. Figure 2 shows details of the flow produced in one of these cases, with a sech^2 density distribution. The run was performed with an initial midplane density equal to 10^6 cm^{-3}, a constant ionizing flux of 5×10^{49} photons s^{-1}, and a scale height $H = 3 \times 10^{16}$ cm (the resulting reference radius was $R_0 = 3.41 \times 10^{16}$ cm and $y_0 = 1.14$). At first, the whole disk becomes fully ionized and begins to expand with the acceleration given in equation (10*b*): the gas velocity increases with height and levels off beyond $z = 2H$. The middle frames show the moment when the midplane density decays to a value of about 4×10^5 cm^{-3}, after a time $t = 1000$ yr, and the ionization front becomes trapped. These values are in fair agreement with the analytical expectations, $n_0(\tau_t) \simeq 5 \times 10^5$ cm^{-3}

and $r_t \simeq 1100$ yr (equations 15 and 16). The third frames show the flow at $t = 3250$ yr. The ionization front is located at about 1.9×10^{17} cm (at the dip in the density distribution), and a shock front is located at 3.8×10^{17} (at the peak of the velocity profile). During the trapping stage, the ionization front recedes towards the origin and becomes trapped within the disk configuration. As the expansion proceeds, less and less mass can be ionized by the diverging radiation field and matter continuously crosses through the ionization front. This gas recombines and cools down to low temperatures, but preserves the momentum acquired during the expansion.

IV.2. Two-dimensional simulations

The evolutionary models in two dimensions were performed with the hydrodynamical code described by Bodenheimer *et al.* (1979). As in the one-dimensional models, the simulations were performed with gaussian, exponential, and sech^2 profiles. For computational purposes, however, in this case the initial density distributions include a halo with constant density. At $t = 0$, the disk-like stratification is held at rest by means of a fake gravitational force (which acts on the flow throughout the evolution), and the low density halo is set in pressure equilibrium with the outer part of the disk. Also, the initial temperature of all gas elements is 10 K. The ionizing source is then placed at the origin of the computational grid, $r = z = 0$, and the hydrodynamical evolution is calculated in only one quadrant. The extent of the ionized region is computed, at every time step, equating photoionizations and recombinations along one hundred different lines of sight from the origin. The photoionized gas is then assumed to attain a temperature $T_{HII} = 8100$ K, unless it has been shocked.

In this latter case, the energy equation accounts for radiative interstellar cooling, and allowed to cool to a minimum temperature of T_{HII}. Outside the ionized volume, the shocked matter is also allowed to cool by radiation, but the minimum temperature here is 10 K.

Figure 3*a* shows the initial condition, immediately after the H II region was formed, for a sech^2 distribution with $n_0 = 10^3$ cm^{-3}, a scale height of 3×10^{16} cm, and $F_* = 10^{43}$ ionizing photons per second. The resulting initial parameters are $R_0 = 2.88 \times 10^{16}$ cm, and $y_0 = 0.96$. The dashed-dotted lines indicate the location of the ionization front and display the initial shape of the H II region. The region becomes unbounded at an angle $\theta_{crit} = 66$ degrees with respect to midplane, in good agreement with the analytical estimates. The sudden change in temperature caused by photoionization leads to pressure gradients and the expansion starts. The rest of the frames in Figure 3 show some details of the expansion.

The largest pressure gradient inside the ionized volume is directed along the z-direction and, as in the one-dimensional calculations, an upward flow develops. The pressure difference between the neutral and ionized gas, on the other hand, generates the sideways expansion of the H II region. This lateral expansion changes the size of the ionized conical volume and drives a rarefaction wave towards the symmetry axis. This wave, in turn, causes the wiggly appearance of the otherwise plane-stratified density distribution. The lateral growth in the halo region proceeds faster than in the disk. This effect is produced by a combination of two processes. The pressure difference at the ionized-neutral interphase drives a shock into the disk and the lateral disk growth proceeds with the well known precursor shock front. The disk expansion, however, allows more photons to reach the halo at increasingly larger azimuthal angles and, as a consequence, the ionization front moves faster in the halo region, and continuously overruns the development of a shock front.

The evolution along the z-axis at early times is similar to the one obtained in the one-dimensional simulations. The upward flow remains until the rarefaction waves set by the lateral expansion have sufficient time to change the direction of the local pressure gradients. This change introduces lateral components and the velocity field begins to acquire a radial appearance. The perturbation begins at the edge of the initial H II region and reaches the symmetry axis at the time $r_{2D} \sim 730$ yr. For $\alpha < y_0 \leq 1$, as in the present case, there exists a trapping stage before r_{2D} (see Section 3.2). Figure 3*c*, at $t = 510$ yr, shows the flow close to the beginning of trapping when the densities at midplane are $\sim 7 \times 10^2$ cm-3, in agreement with the analytical predictions (equations 15 and 16). Note that the trapping begins at an angle from the symmetry axis, which corresponds to the section that is still unaffected by the pasage of the rarefaction waves, and reaches the axis in short time (Fig. 3*d*). The geometrically diverging photon flux is absorbed by recombinations within the expanded disk and the ionization front rapidly receeds towards the star. The ionized region there attains a size $\sim 7 \times 10^{17}$ cm, slightly larger than the size along midplane. After r_{2D} the rarefaction waves lead to the depletion of the original column density even at the most inner parts of the H II region and the ionization front is capable of ionizing once more all material up to the edge of the computational grid (see last frame Figure 3). The phenomena lasted only about two hundred years and will not be repeated as long as the expansion maintains a diverging flow.

V. SUMMARY AND CONCLUSIONS

The evolution of H II regions in disk-like clouds, with and without magnetic fields, presents several

interesting properties. Some details depend on the particular density profile, but the main features are determined by the scale height and the initial Strömgren radius along midplane. As discussed in Paper I, the initial shape of the ionized region has a critical point, $y_0 = \alpha$, which defines a fully ionized conical section in the disk.

For initially unbounded regions, $y_0 > \alpha$, the gas flows mainly directed along the z-axis and the initial acceleration is proportional to the inverse of the scale height. Thus, regardless of the values in midplane densities, highly flattened disks can produce large expansion velocities. As long as the column densities are held nearly constant, the expanded disk can trap the ionization front and the H II region becomes bounded. If a B-field oriented parallel to the z-axis is present, the event is long lasting and causes the appearance of a supersonic neutral outflow. The mass and momentum of the supersonic neutral gas depend on the specific details of the disk and ionization source, but cases with $y_0 > 1$ are likely to generate powerful outflows. Otherwise, in the absence of magnetic fields, the lifetime of the trapping stage is limited by two-dimensional effects. Detailed hydrodynamical simulations of the evolution have provided additional features of the event. The trapping begins off-axis, where the column densities are larger, and reach the symmetry axis in a very short time. In addition, a shock front develops near the trapping time and runs into the recently formed neutral outflow.

The connection of these results to some of the outflows already detected in star forming regions seems appealing. There is growing evidence for the existence of disk-like structures associated with recently formed objects (e.g., Torrelles *et al.* 1983; Harvey 1985; Kenyon and Hartmann 1987), and there are compact H II regions associated with high-velocity H I outflows (e.g., Russell 1987). These two features can be causally related in a model with trapped ionization fronts and its application to particular objects will be explored in a future work.

We thank H. U. Schmidt for useful comments on the manuscript. T. Hartquist provided many challenging questions at the early stages of this study and R. Genzel has been playing the devil's advocate. P. B. and J. F. acknowledge the hospitality of the Max-Planck Institut für Astrophysik. J. F. acknowledges partial financial support from CONACyT-México. G. T.-T. is supported by the Deutsche Forschungsgemeinschaft grant M0416.

REFERENCES

Bodenheimer, P., Tenorio-Tagle, G., and Yorke, H. W. 1979, *Ap. J.*, **233**, 85.

Bodenheimer, P., Yorke, H. W., Tenorio-Tagle, G., and Beltrametti, M. 1983, in *Supernova Remnants and Their X-Ray Emission, IAU Symp. 101*, eds. J. Danziger and P. Gorestein (Dordrecht: Reidel Publ. Co.), p. 399.

Franco, J., Tenorio-Tagle, G., and Bodenheimer, P. 1989, to *Ap. J.*(Paper I), in press.

Harvey, P. M. 1985, in *Protostars and Planets II*, eds. D. C. Black and M. S. Matthews (Tucson: Univ. Arizona Press), p. 484.

Kenyon, S. J., and Hartmann, L. 1987, *Ap. J.*, **323**, 714.

Lizano, S. 1989, *Rev. Mex. Astron. Astrof.*, in press.

Osterbrock, D. E. 1989, *Astrophysics of Gaseous Nebulae and Active Galactic Nuclei*, (Mill Valley: University Science Books).

Russell, A. P. G. 1987, *Ph. Thesis*, University of Cambridge, U. K.

Tenorio-Tagle, G., Bodenheimer, P., Lin, D. N. C., and Noriega-Crespo, A. 1986, *M. N. R. A. S.*, **221**, 635.

Torrelles, J. M., Rodriguez, L. F., Cantó, J., Carral, P., Marcaide, J., Moran, J. M., and Ho, P. T. P. 1983, *Ap. J.*, **274**, 214.

Peter Bodenheimer: Lick Observatory, University of California, Santa Cruz, CA 95064, USA.

José Franco: Instituto de Astronomía, UNAM, Apartado Postal 70-264, 04510, México, D.F., México.

Guillermo Tenorio-Tagle: Max-Planck Institut für Astrophysik, D-8046 Garching bei München, F.R.G.